

Article

New Reactive Power Compensation Strategies for Railway Infrastructure Capacity Increasing

Vítor A. Morais ^{1,*}, João L. Afonso ², Adriano S. Carvalho ¹ and António P. Martins ¹

¹ Department of Electrical and Computers Engineering, University of Porto, 4200-465 Porto, Portugal; asc@fe.up.pt (A.S.C.); ajm@fe.up.pt (A.P.M.)

² Centro ALGORITMI, University of Minho, 4800-058 Guimarães, Portugal; jla@dei.uminho.pt

* Correspondence: v.morais@fe.up.pt

Received: 31 July 2020; Accepted: 23 August 2020; Published: 25 August 2020



Abstract: In AC railway electrification systems, the impact of reactive power flow in the feeding voltage magnitude is one aspect contributing to the quality of supply degradation. Specifically, this issue results in limitations in the infrastructure capacity, either in the maximum number of trains and in maximum train power. In this paper, two reactive power compensation strategies are presented and compared, in terms of the theoretical railway infrastructure capacity. The first strategy considers a static VAR compensator, located in the neutral zone and compensating the substation reactive power, achieving a maximum capacity increase up to 50% without depending on each train active power. The second strategy adapts each train reactive power, achieving also a capacity increase around 50%, only with an increase of the train apparent power below 10%. With a smart metering infrastructure, the implementation of such compensation strategy is viable, satisfying the requirements of real-time knowledge of the railway electrification system state. Specifically, the usage of droop curves to adapt in real time the compensation scheme can bring the operation closer to optimality. Thus, the quality of supply and the infrastructure capacity can be increased with a mobile reactive power compensation scheme, based on a smart metering framework.

Keywords: electric traction systems; mobile reactive power compensation; power quality; railway power systems; railway infrastructure capacity; smart railways

1. Introduction

The Railway transportation system has huge power requirements, leading the railway operators to be focused on the increase of the energy efficiency in order to reduce the energy consumption bill. According to [1], the railway sector has a 9% market share in transportation of passengers and goods in the European Union, with an increase of 8.9% between 2005 and 2015. In addition, this market share is only achieved with a final energy consumption of 2%, in comparison with other sectors.

With the mission of “Moving European Railway Forward”, the Shift2Rail European program [2] targets the reduction of costs, increases the capacity, reliability, and punctuality. In particular, this program contributes to doubling the railway capacity [3].

The increase of railway infrastructure capacity is an extensive research area where the evaluation is made with the application of definitions, metrics methodologies, and tools [4]. Despite there being no standard definition of railway capacity, it can be defined as the number of trains that can safely pass over a segment of line, within a selected time period.

Regarding the electrification aspects, generally the railway infrastructure capacity is directly affected by the current collection quality of the electric train, which is normally determined by both the mechanical and electrical parts. The mechanical part concerns the train–infrastructure interactions, like pantograph-catenary [5,6], and the wheel-rail [7], which determines the stability of

electric transmission and is a source of electrical issues. Due to the inductive characteristic of railway transmission line, this will directly affect the quality of supply of electric trains, being also a source of electrical issues.

Specifically, due to the electrical characteristics of the railway electrification, the increase of railway infrastructure capacity leads to an increase in line voltage drop. According to the IEC60850 [8], in AC 1×25 kV electrification scheme, the lowest non-permanent voltage is 0.7 p.u. (17.5 kV), whereas the lowest permanent voltage is 0.76 p.u. (19 kV). Specifically, if the voltage is higher than the lowest permanent voltage, the train can consume all its demand power; if the lowest non-permanent voltage is reached, a limit of operation is achieved and the train power must be clipped to zero.

It is well known that the higher the reactive power flow, the higher the voltage drop across the catenary line [9]. The study of reactive power, and power flow depends on a model for the catenary.

The catenary line is usually modeled as a multi-conductor line model, for each of the conductors (rails, buried cables, aerial protection cables, feeder cables, and contact line, as example). This results in a matrix of self and mutual impedances, where the main diagonal (self impedance) depends on the analysis of the ring formed by the respective conductor and the earth return, and the remaining elements of the matrix corresponds to the mutual impedances [10]. These elements can be obtained from the application of the Carson formulas, as proposed in [11] and as demonstrated its railway application in [12].

For power flow calculations and for 1×25 kV electrification scheme, the multi-conductor line model can be simplified to consider the same voltage level in the conductors. First, the earth conductance is not considered, as well as the rail–earth conductance and the capacitance matrix. Therefore, this can be simplified to a lumped-parameters line model. As illustrated in [12], one approach to perform this simplification is in adding all the admittance matrix elements corresponding to the same voltage level. For 1×25 kV, this results in a 2×2 impedance matrix that can be further simplified to a PI model.

This simplified model allows a proper usage of common power flow solvers in the railway electrification analysis, namely reactive power flow control. This paper proposes an adaptation on the railway reactive power control, towards an increase in the railway infrastructure capacity. This adaptation will directly result in a reduction of the losses, as a first objective, bringing clear advantages to the railway infrastructure.

This paper is structured in seven sections. The following Section 2 presents a literature review. Section 3 presents the materials and models, starting with a basic model and covering the used simulation framework. Section 4 presents the methodology for reactive power compensation, with an illustration for a particular scenario. Section 5 presents the rest of the methodology and the results for the increase in the railway infrastructure capacity with the adaptation of the reactive power in the catenary. Section 6 discusses a conceptual architecture to implement this reactive power compensation strategy, with the usage of a smart metering framework. Finally, the conclusions of this work are presented in Section 7.

2. Literature Review

Several works have been addressed in the literature regarding strategies for power quality improvement in railways. In AC electrification, two main types of devices based on power electronics are usually implemented: voltage stabilization devices, or voltage boosters, and line current balancers [13].

The main objective of the high voltage boosters is to inject reactive power into the line, with a level adapted in real time. Usually, this is achieved with a static VAR compensator (SVC) and tuned LC filters for specific harmonics [13].

The purpose of line current balancers is to minimize the unbalance caused in the transmission/distribution network by the railway electrification.

These two types of devices are necessary to comply with the increase for power demand. Usually, infrastructure managers adopt systems in the Traction Power Substation (TPS) site that can either balance the line currents and inject reactive power (to boost the catenary voltage).

In [14,15], comparative studies on several Railway Power Conditioners (RPC) topologies are presented, to be employed in the TPS. Traditional RPC comprises two back-to-back converters and two isolation/coupling transformers [16,17]. From this topology, several have been derived, such as the active power quality compensator (AQPC) which comprises a three phase converter [18], or the hybrid power quality compensator (HPQC) in which the APQC is combined with a Static VAR compensator [19,20]; In addition, modular multilevel converter (MMC) topologies have been researched in current years [21].

Despite the inability to control the line current unbalances, the inclusion of voltage stabilization devices in the opposite site of the TPS (in the end of a traction feeder section, the neutral zone) will strongly support this desired voltage boost. Thus, this compensation strategy allows more powerful trains without violating the standards (e.g., IEC60850 [8]). In [22,23], strategies are presented to include compensation systems at the end of a traction section feeder. In [24], the 3 kV increase in the minimum voltage in the catenary is highlighted, with further details of this project in [25]. However, this improvement is achieved with a system occupying a very large area. The compensation scheme for Static VAR Compensator is also studied in [26], with the usage of a neural network for online operation.

In the PhD thesis of [27] and later in [28], an alternative to the inclusion of bulky SVCs is proposed, with the adoption of mobile reactive power compensators. This is achieved with the reactive power injection within each train. This compensation strategy is further extended with the work of [29], where the compensation scheme is based in a genetic algorithm heuristic. Later in [30], the usage of modern locomotives as mobile reactive power compensators is evaluated and compared, where they can be more efficient than SVC. However, the limitations related to the control of leading power factor as well as the need for very fast algorithms are considered that do not justify the usage of a power factor different than the unitary.

From the knowledge of the authors, the possibility of operating the modern trains with variable power factor has not been actively researched in recent years. However, from the authors' point of view, the reason for this is not in the advantages, but in the difficulty to implement such a strategy, since it requires real-time knowledge of the state of the railway electrification.

Regarding the infrastructure capacity increase, most works are focused on the operational and logistics. In [31], the main concepts and methods to perform capacity analysis are reviewed. In theory, the capacity is defined as the number of trains running over a line section, during a time interval, with trains running at minimum headway. This capacity mostly depends on infrastructure constraints (signaling system, power traction constraints, single/double tracks, speed limits, etc.), on traffic parameters (timetables, priorities, type of trains, etc.) and on operation parameters (track interruptions, train stop time, etc.). In [3], increasing the railway infrastructure capacity by increasing the speed of freight trains is proposed. Specifically, in the case of a delay, these trains are allowed to have higher maximum speed.

In this work, the infrastructure capacity increase with the adoption of reactive power compensation strategies is reviewed. In the following section, the models and the used framework to demonstrate the infrastructure capacity improvement are presented.

3. Materials and Methods

This section covers the models and simulation framework required for power flow analysis and for reactive power control. The combination of these models, the simulation framework, and the compensation strategy will be the scientific contribution for a new approach to reactive power control in the railway system.

3.1. Basic Model

The basic model considers the Traction Power Substation (TPS), the catenary line, and the electric train. The electric train is simplified from the dynamic model as follows:

$$\frac{dv}{dt} = \frac{F_T(v) - w(v) - g(x)}{M(t)} \quad (1)$$

where $F_T(v)$ is the traction force, $w(v)$ is the aerodynamic resistive force, and $g(x)$ represents the track gradient and curvature forces. The electric active power is directly related to the train dynamic movement and the reactive power is the one to control. At higher speeds, the maximum traction force is limited by the maximum available power [32]. Therefore, the train can be simplified to a decoupled active and reactive power load.

In this work, the considered line model is represented as the PI line model, Z_L . Then, the railway power flow can be analyzed in Figure 1, where the train, V_t , is supplied through the catenary line, Z_L , from a 25 kV TPS, V_s .

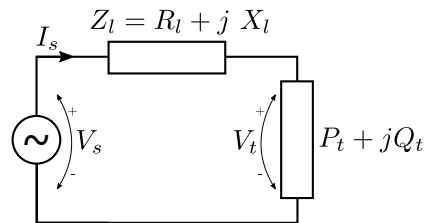


Figure 1. Steady state equivalent circuit.

The apparent, active, and reactive power flows (S_s , P_s and Q_s , respectively) in the TPS can be obtained from the following expressions:

$$\begin{aligned} S_s &= V_s I_s^* \\ &= P_s + jQ_s \end{aligned} \quad (2)$$

The current in the branch can be expressed as:

$$I_s = \frac{\hat{V}_s - \hat{V}_t \cos(\delta) - j \hat{V}_t \sin(\delta)}{R_l + jX_l} \quad (3)$$

where $V_s = \hat{V}_s \angle 0$ and $V_t = \hat{V}_t \angle \delta$. Thus, replacing the expression in (2),

$$\begin{aligned} P_s &= \frac{\hat{V}_s^2 R_l - \hat{V}_s \hat{V}_t R_l \cos(\delta) - \hat{V}_s \hat{V}_t X_l \sin(\delta)}{R_l^2 + X_l^2} \\ Q_s &= \frac{\hat{V}_s^2 X_l + \hat{V}_s \hat{V}_t R_l \sin(\delta) - \hat{V}_s \hat{V}_t X_l \cos(\delta)}{R_l^2 + X_l^2} \end{aligned} \quad (4)$$

It can be seen that the active and reactive power flow in the TPS is dependent on the magnitude and phase of the train voltage, as well as on the line characteristics.

Supported by the expression in (4), let's consider a variation of the train voltage magnitude (from 15 kV to 30 kV) and the train voltage phase (between $-\pi/4$ to $\pi/4$). Assuming a line distance of 30 km and $X/R = 3$, Figure 2 shows the TPS active and reactive power as a function of the train voltage and phase.

The lines in Figure 2 show the isobaric lines where the power flow at TPS is the same. In particular, in each figure, the lines having, respectively, 0 MW for Figure 2a and 0 MVar for Figure 2b is highlighted.

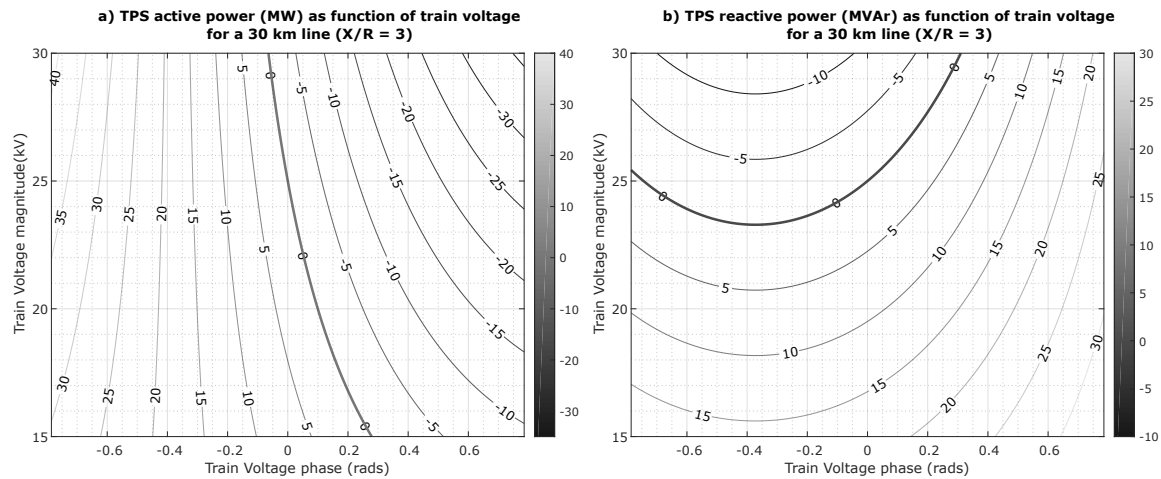


Figure 2. Sensibility analysis for different conditions of train voltage and phase: (a) Active power flow at TPS; (b) Reactive power flow at TPS.

From the analysis of Figure 2a, it is possible to view that a variation on the phase of the train will considerably affect the active power flow in the TPS (the variation of the train voltage is barely related to a variation on active power flow at TPS).

Regarding Figure 2b, it is visible that, for a train voltage phase angle of, around, -0.4 radians, the reactive power only depends on the train voltage.

If the train active and reactive power is obtained from the application of previous sensibility analysis, it is possible to perform a correlation of TPS power flow and train power flow. Specifically, the train power is given by:

$$P_t + jQ_t = V_t I_s^* \quad (5)$$

Replacing the I_s^* by expression in (3), it is obtained for P_t and Q_t the following:

$$P_t = \frac{\hat{V}_t \hat{V}_s R_l \cos(\delta) + \hat{V}_t \hat{V}_s X_l \sin(\delta) - \hat{V}_t^2 R_l \cos(2\delta) - \hat{V}_t^2 X_l \sin(2\delta)}{R_l^2 + X_l^2} \quad (6)$$

$$Q_t = \frac{\hat{V}_t \hat{V}_s R_l \sin(\delta) - \hat{V}_t^2 R_l \sin(2\delta) + \hat{V}_t^2 X_l \cos(2\delta) - \hat{V}_t \hat{V}_s X_l \cos(\delta)}{R_l^2 + X_l^2}$$

The TPS active and reactive power can be related to the train power, through a variable change. However, considering the expressions in (4) and (6), there is no simple mathematical solution that results in the TPS power as function of the train power.

A simple procedure (to conduct a variable change of the train voltage and phase, in order to obtain the TPS power, from expression (4), and the train power, from expression (6)), towards an evaluation of the dependence of TPS power from the train voltage is considered. The result of this evaluation can be analyzed graphically, in Figure 3.

Figure 3a presents isobaric curves of active power at TPS, as a function on the train active and reactive power. In particular, in this result, it is visible that TPS active power is more dependent on train active power. In Figure 3b, the dependence of TPS reactive power is more dependent on the train reactive power.

To conclude, in previous analysis, a dependence on TPS reactive power and train voltage magnitude are visible. Specifically, by having an inductive reactive power flow in the TPS, the train voltage magnitude will reduce, as visible in Figure 2a. In addition, by changing the train reactive power value, this results in an adaptation of the reactive power in the TPS.

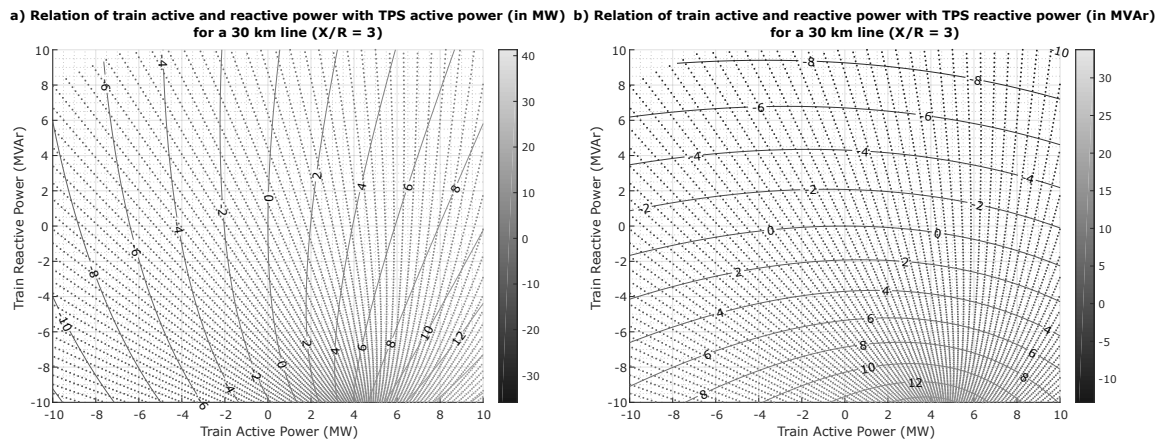


Figure 3. Sensibility analysis for different conditions of train power: (a) active power flow at TPS; (b) reactive power flow at TPS.

Thus, the adaptation of the reactive power by changing the train reactive power to a capacitive power factor results in a reduction of the TPS reactive power and an increase of the train voltage level.

3.2. Simulation Framework

The simulation framework of this work is now presented in Figure 4, where the TPS, a railway line, and a single train are illustrated.

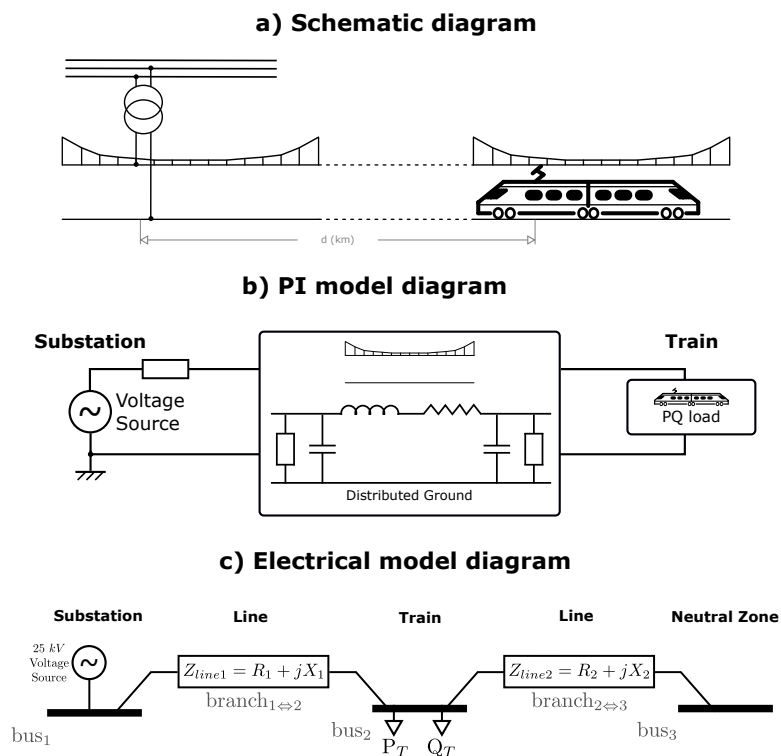


Figure 4. Framework of the 1×25 kV models: (a) illustration of physical representation; (b) PI model diagram; (c) considered bus-branch model for MatPower (Note: the traction transformer is not considered in this work).

The power flow problem considered in this simple model is a nonlinear problem, as previously discussed. The usage of MatPower [33], and, in particular, the Newton–Raphson solver, allows this problem to be solved. Therefore, for a fixed supply voltage and specific branch parameters, the train

power consumption can be fixed regardless of the voltage drop in the line. With this, the voltages in the nodes can be calculated, as well as the injected supply power in the TPS.

Considering the simple model in Figure 4c, this has four variable parameters: (i) a variable line distance, d_L ; (ii) a variable train power, P_T ; (iii) a variable train power factor, PF_T ; and (iv) a variable line X/R ratio, X/R_L .

To better evaluate the model, these parameters can be spawned across a surface of possible parameters $S(L_d, X/R_L, P_T, PF_T) \in \mathbb{R}^4$, where $d_L \in]0 \ d_{max}]$, $X/R_L \in [X/R_{min} \ X/R_{max}]$, $P_T \in [P_{min} \ P_{max}]$ and $PF_T \in [0 \ 1]$. The surface of possible parameters has infinite possible solutions.

One element of the surface of parameters can be parametrized as set of parameters $SP(L_d, X/R_L, P_T, PF_T) \in S$, where

$$\text{Set of parameters } SP = \begin{cases} L_d & (\text{in km}) \\ X/R_L & \\ P_T & (\text{in MW}) \\ PF_T & \\ \text{Voltage @ bus}_k & k = \{1, 2\} \\ \text{Power bus}_k & k = \{1, 2\} \\ \text{Line losses} & P \text{ and } Q \end{cases} \quad (7)$$

To study the behavior of this model, it is possible to generate several SP elements, using distribution probability function for each of the four parameters, inside the defined interval of values. Assuming that, for each parameter, N random possibilities are generated. Then, the surface of solutions depends on testing N^4 different elements, resulting in a huge computational power required for this model and a hard task to evaluate the model. A more direct analysis, in particular, a sensibility analysis, will better illustrate and validate the behavior of the model.

3.3. Sensibility Analysis

A sensibility analysis is an adequate tool to evaluate the variation of certain input variables, in particular, the variation of the parameters. In this analysis, three parameters can be defined as variable and the fourth can be fixed, as better explained in the following results.

Considering a testing surface, given by the expression:

$$S = \begin{cases} L_d & [0.1 : 2 : 30.1] \quad (\text{in km}) \\ X/R_L & \{2 : 1 : 5\} \\ P_T & [-20 : 2 : 20] \quad (\text{in MW}) \\ PF_T & \{0.8 \ 0.9 \ 0.95 \ 1\} \quad \text{ind.} \end{cases} \quad (8)$$

By fixing the X/R_L ratio, then this leaves room to variate the other three variables. Thus, the sensibility analysis can be seen within the train voltage value, as visible in Figure 5.

Complementarily, the second sensibility analysis is made by fixing the PF_T value. The remaining parameters will be variate towards an evaluation of the resultant voltage value, as visible in Figure 6.

From the evaluation of the parameters of the model, it is clear that the X/R_L ratio will affect the train voltage. Specifically, a higher X/R_L ratio results in higher voltage drops in the line, which is a characteristic of high inductive lines. Nevertheless, the characteristics of the line depend on several aspects related to the design of the electrification, and, therefore, in this work, a fixed value for the X/R_L ratio (specifically, $R_L = 0.15 \ \Omega/\text{km}$ and $X_L = 0.45 \ \Omega/\text{km}$) is considered.

The only aspect that can be manipulated is the train power factor. By having higher power factor values, this reduces the voltage drop. Therefore, in the following section, the reactive power compensation is detailed.

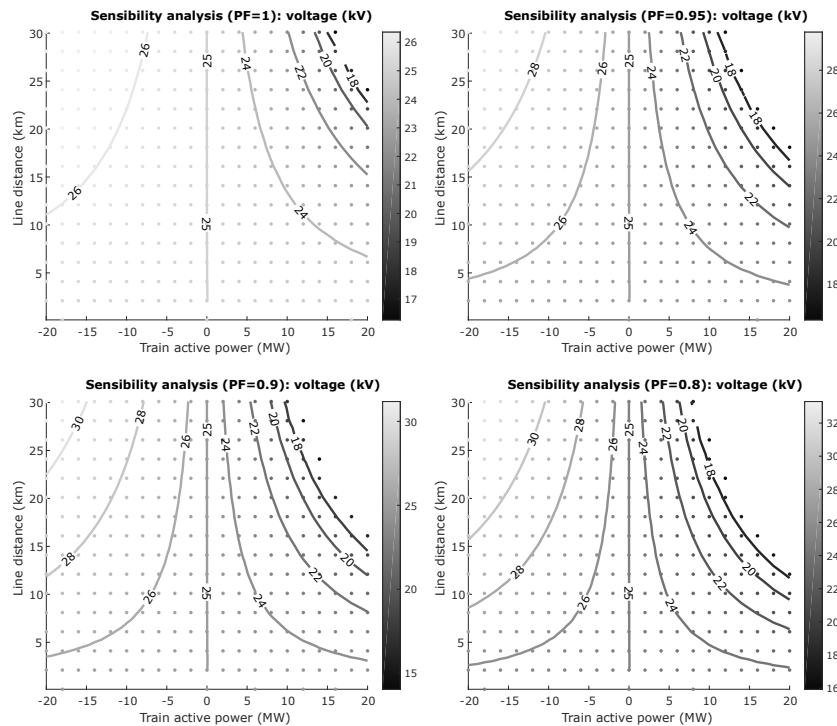


Figure 5. Sensibility analysis for $X/R_L = 3$: voltage levels for different train power factor values, spawned across different train active power values and line distances.

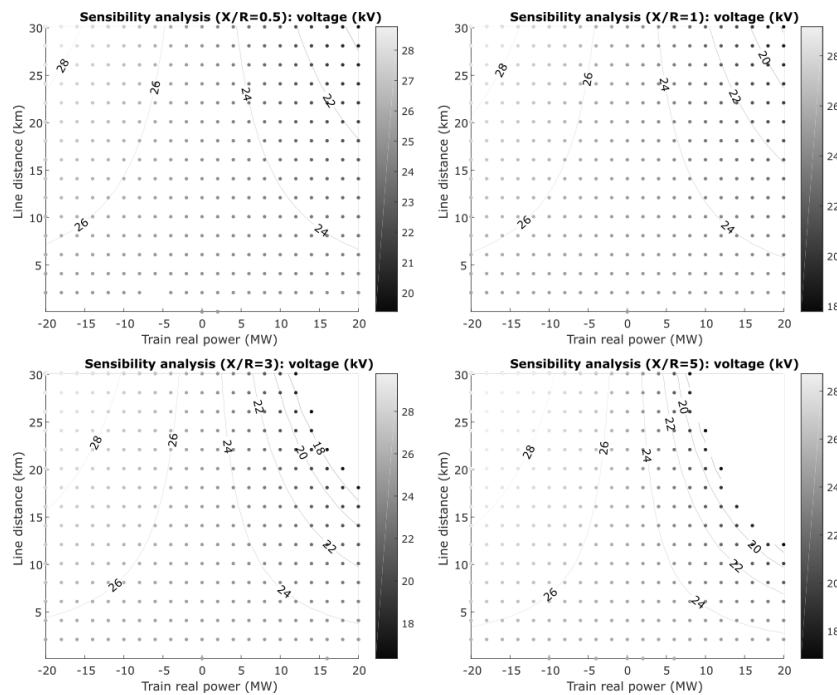


Figure 6. Sensibility analysis for $PF_T = 0.95$: voltage levels for different X/R_L ratios.

4. Reactive Power Compensation

As previously illustrated, there is a clear advantage in controlling the reactive power in the railway electrification. This section covers the used methodology to improve the traction power supply with the adaptation of the train power factor, using references coming from measurements from TPS. In this section, a simple reactive power compensation algorithm is presented first, and is demonstrated in the performance of such algorithm.

4.1. Algorithm for Reactive Power Compensation

The adopted optimization strategy was based on the compensation strategy from [27], where the train reactive power is iteratively adapted, based on solving the power flow problem. This simple algorithm is presented in the following Algorithm 1, based on fixed steepest descent method, where Q_{MIN} is a tolerance value for the reactive power and the λ is the step size for the iterative process.

Algorithm 1: Reactive Power Compensation Using Fixed Steepest Descent Method

```

1 begin
2   SET  $Q_k = 0\text{Mvar}$ ;
3   SET  $\lambda = \lambda_0$ 
4   while NOT termination criteria do
5     LAUNCH (Power Flow Algorithm)
6     GET  $Q_{SST}$ 
7     if  $|Q_{SST}| \geq Q_{min}$  then
8       SET  $Q_{k+1} = Q_k - \lambda Q_{SST}$ 
9     else
10      BREAK
11    end
12  end
13 end

```

Considering the following set of parameters SP , where

$$SP = \begin{cases} L_d = 30 \text{ km} \\ X/R_L \approx 3 \\ P_T = 10 \text{ MW} \\ PF_T = 0.90 \text{ ind. (initial value)} \end{cases} \quad R = 0.155 \Omega/\text{km} \quad (9)$$

Figure 7 presents the results for the proposed algorithm (with fixed $\lambda_0 = 0.25$), for the optimization of SP .

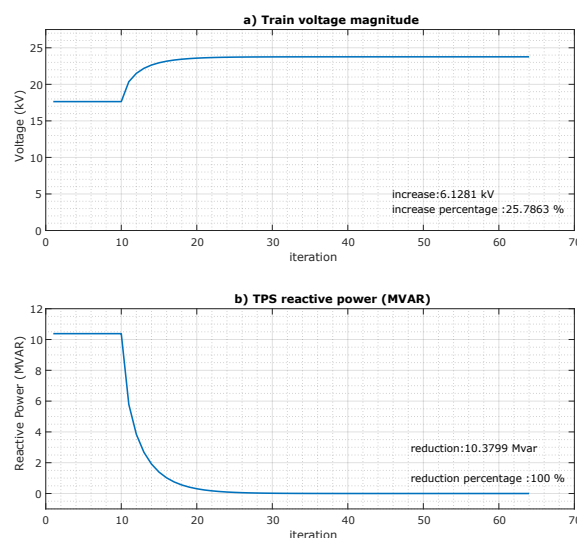


Figure 7. Illustration of algorithm evolution for reactive power compensation: (a) evolution of train voltage; (b) evolution of SST reactive power. Note, for illustration purposes, that the reactive compensation procedure is only enabled at iteration $it = 10$.

This result clearly illustrates the major advantages of this reactive power compensation. The train voltage increases 25.8%, and the resultant reactive power in traction substation is zero.

Regarding the train operation, as illustrated in Figure 8, the train active power consumption is unaffected, as expected; the reactive power is considerably changed, from an inductive power factor to a capacitive one; the big advantage is on the reduction of the apparent power consumption which is directly related to a reduction in train power losses (in train transformer and power converters).

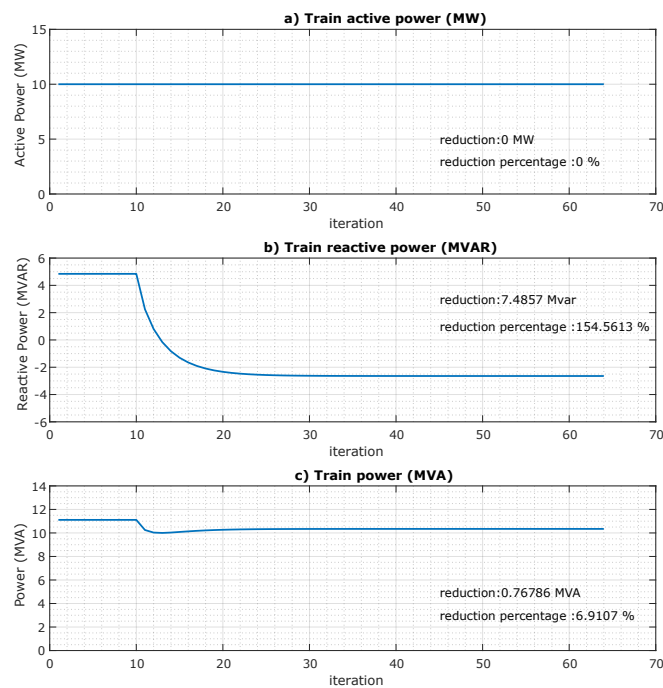


Figure 8. Illustration of algorithm evolution for reactive power compensation: (a) evolution of train active power; (b) evolution of train reactive power; (c) evolution of train apparent power.

Finally, the major advantage of this strategy is visible in Figure 9, where the power losses in catenary can be reduced by half.

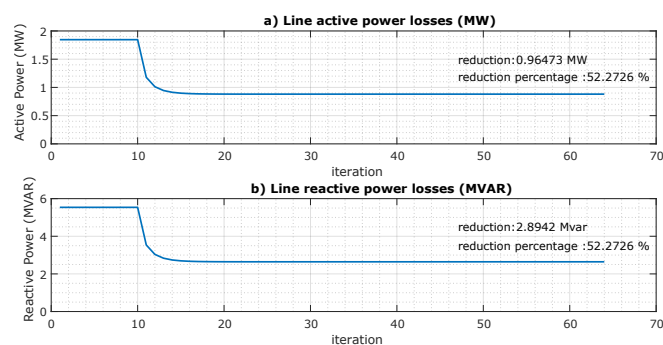


Figure 9. Illustration of algorithm evolution for reactive power compensation: (a) evolution of active power losses in catenary; (b) evolution of reactive power losses in catenary.

However, these results must be taken with caution, regarding the predefined parameters and specifically the initial inductive train power factor of 0.9. In the following, a sensibility analysis will be made to better evaluate the potential improvement from initial different power factors.

4.2. Sensibility Analysis

Figure 9 presents the visible active and reactive power losses in the catenary, for SP in (9). A sensibility analysis will be performed for a fixed $X/R_L \approx 3$, with the results in Figure 10.

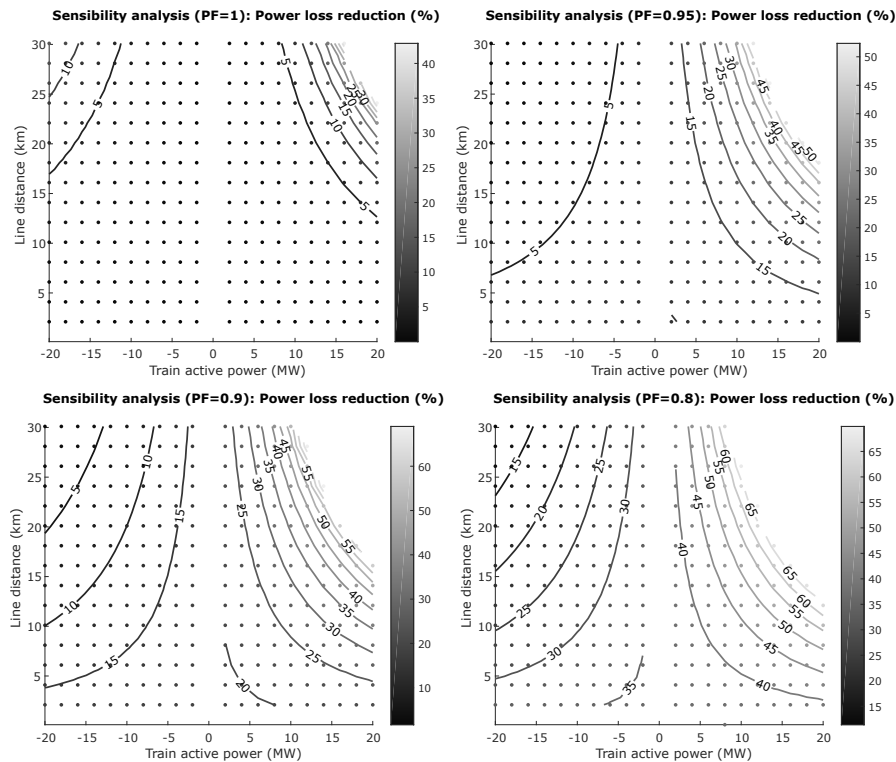


Figure 10. Sensibility analysis for reactive power compensation: line power loss reduction, in percentage, for different power factors. Note that the values near 0 MW or near 0 km are not relevant for this demonstration.

As expected, for lower values for PF_T , this results in higher reduction in the line losses. This value is expected since trains will have more margin to adapt the power factor value to a capacitive one.

In the following section, this algorithm will be included to compensate the reactive power in two situations: (i) compensation in NZ through a PWM controlled SVC, using measurements from TPS; and (ii) compensation made by each train.

5. Increase of the Railway Infrastructure Capacity

This section proposes to increase the infrastructure capacity of a railway line (increase of the number of trains), with the adoption of a reactive power compensation strategy.

The railway infrastructure capacity will be considered, in this section, as the maximum number of trains that can exist in a railway line, all of them separated with the same distance among each others, and that the voltage levels on the line are according to IEC60850 [8]. The security issues such as minimum distance that a train must be apart from each other will not be considered.

Consider a railway line branch, with fixed length separating the TPS and a neutral zone, and having N trains. In order to better evaluate the infrastructure capacity, in the implemented model illustrated in Figure 11, the distances d_1, d_2, \dots, d_{n+1} are all the same, as well as all the train powers, P_T and Q_T .

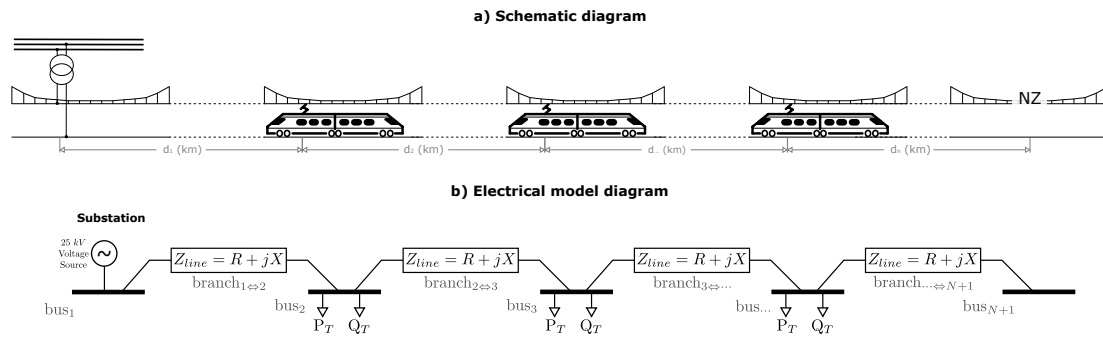


Figure 11. Framework for the increase of railway capacity: (a) illustration of physical representation; (b) considered bus-branch model for MatPower.

With this consideration, three different case studies can be listed:

- Study of railway capacity without compensation (Baseline);
- Installation of a Static VAR Compensator located at neutral zone;
- On-board compensation in all trains;

5.1. Baseline: Railway Capacity without Compensation

This section takes into account a railway line having a fixed length $D_{TPS \leftrightarrow NZ} = 29.2$ km (corresponding to the maximum distance of a track section of a real 250 km railway line, from the knowledge of the authors).

The procedure to evaluate the railway capacity is illustrated in Figure 12, where the addition of trains to the railway line is iteratively tested.

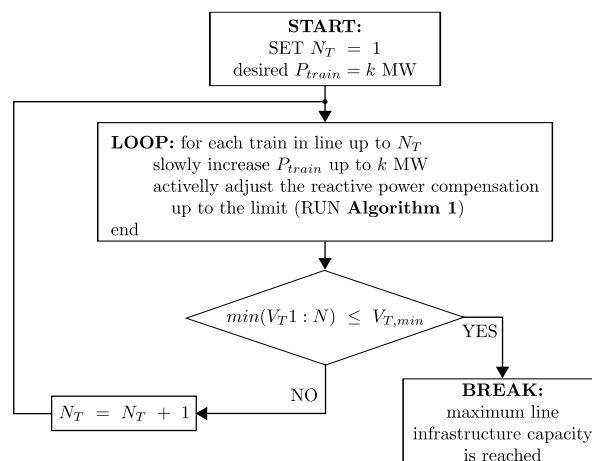


Figure 12. Flowchart to test the increasing of capacity procedure.

Specifically, considering that the line has N trains, each train will be separated among them by a fixed distance:

$$d_T = \frac{D_{TPS \leftrightarrow NZ}}{N + 1} \quad (10)$$

It is noteworthy that the usage of variable train distances will result in opening a degree of freedom that, only with an extensive probabilistic analysis (for different distances), is it possible to obtain reasonable results. Nevertheless, similar results are expected.

In this baseline case study, the procedure in Figure 12 will not consider the active adjustment of reactive power. The maximum infrastructure capacity is then achieved when the voltage in the line is lower than the IEC60850 minimum non-permanent voltage (17.5 kV [8]). The decision for choosing the non-permanent voltage was arbitrary between the two minimum IEC60850 voltage limits (both

voltage level values are valid for the following analysis, expecting similar results; the window between these two levels must not be considered as a steady state train operation).

Figure 13 illustrates the results, where a relation of the number of trains and the minimum voltage level is illustrated for different cases.

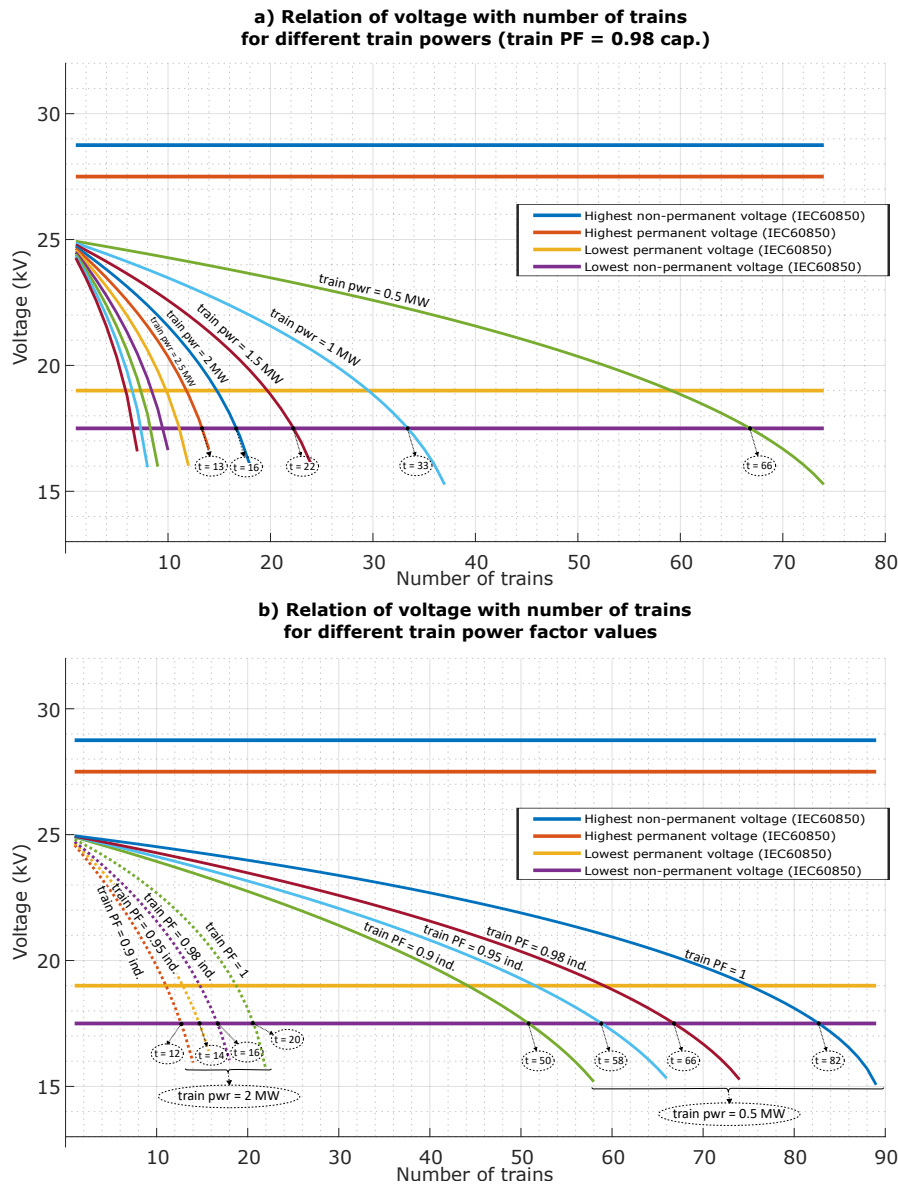


Figure 13. Relation of number of trains with voltage in neutral zone: (a) variation of active power in each train, for fixed $PF = 0.98$ ind.; (b) variation of power factor in each train, for fixed active power of 0.5 MW and 2 MW.

Specifically, Figure 13a presents the dependence of minimum voltage level and the number of trains, for different power values in each train. In theory, it is possible to have 16 trains in the line, all consuming 2 MW with $PF = 0.98$ ind., without achieving the lower value of non-permanent voltage (17.5 kV according to IEC60850).

Figure 13b shows the voltage for different train power factors, where the increase to unitary power factor from $PF = 0.9$ ind. results in an increase of the railway capacity around 67% (for $P_t = 2$ MW, increase from 12 to 20 trains).

Table 1 extends the evaluation of railway capacity for different train power consumptions and for different train power factors.

Table 1. Maximum number of trains, for different train power consumptions and for different train power factors. Note: the percentage reduction from unitary power factor is presented in parentheses. As an example, the baseline for $P_T = 2$ MW and $PF = 1$ is 20 trains; then, for $PF = 0.9$ ind., it is only possible to have 12 trains (8 less than the unitary power factor, corresponding -40% less than baseline).

Train Active Power	Train Power Factor			
	0.9 ind.	0.95 ind.	0.98 ind.	1
0.5 MW	50 (−39.0%)	58 (−29.3%)	66 (−19.5%)	82 (0%)
1 MW	25 (−39.0%)	29 (−29.3%)	33 (−19.5%)	41 (0%)
2 MW	12 (−40.0%)	14 (−30.0%)	16 (−20.0%)	20 (0%)
3 MW	8 (−38.5%)	9 (−30.8%)	11 (−15.4%)	13 (0%)
4 MW	6 (−40.0%)	7 (−30.0%)	8 (−20.0%)	10 (0%)
5 MW	5 (−37.5%)	5 (−37.5%)	6 (−25.0%)	8 (0%)

From this baseline, two possible strategies for the railway reactive compensation will be covered, considering each train starting with $PF = 0.98$ ind.

5.2. Reactive Power Compensation in the Neutral Zone

In the second case study, the reactive power compensation will be made with a SVC in the neutral zone, having the objective of minimizing the SST reactive power. Figure 14 presents the lower voltage in line, as a function of the number of trains in the line.

Table 2 extends the evaluation of railway capacity for different power consumptions and for different compensation limits at the neutral zone.

Table 2. Maximum number of trains, for different train power consumptions and for different Neutral Zone power limits. Note: the percentage improvement from baseline is presented in parentheses (where 0 MVar means no compensation). As an example, the baseline for $P_T = 2$ MW is 16 trains; then, for $Q_{NZ} = 20$ MVar, it is possible to have nine more trains ($+56\%$ more than baseline).

Train Active Power	Neutral Zone Power Limit (for Compensation)				
	0 MVar	5 MVar	10 MVar	20 MVar	30 MVar
0.5 MW	66 (0%)	81 (+22.73%)	90 (+36.36%)	100 (+51.52%)	105 (+59.09%)
1 MW	33 (0%)	40 (+21.21%)	45 (+36.36%)	50 (+51.52%)	52 (+57.58%)
2 MW	16 (0%)	20 (+25%)	22 (+37.50%)	25 (+56.25%)	26 (+62.50%)
3 MW	11 (0%)	13 (+18.18%)	15 (+36.36%)	16 (+45.45%)	17 (+54.55%)
4 MW	8 (0%)	10 (+25%)	11 (+37.50%)	12 (+50%)	12 (+50%)
5 MW	6 (0%)	8 (+33.33%)	8 (+33.33%)	9 (+50%)	10 (+66.67%)

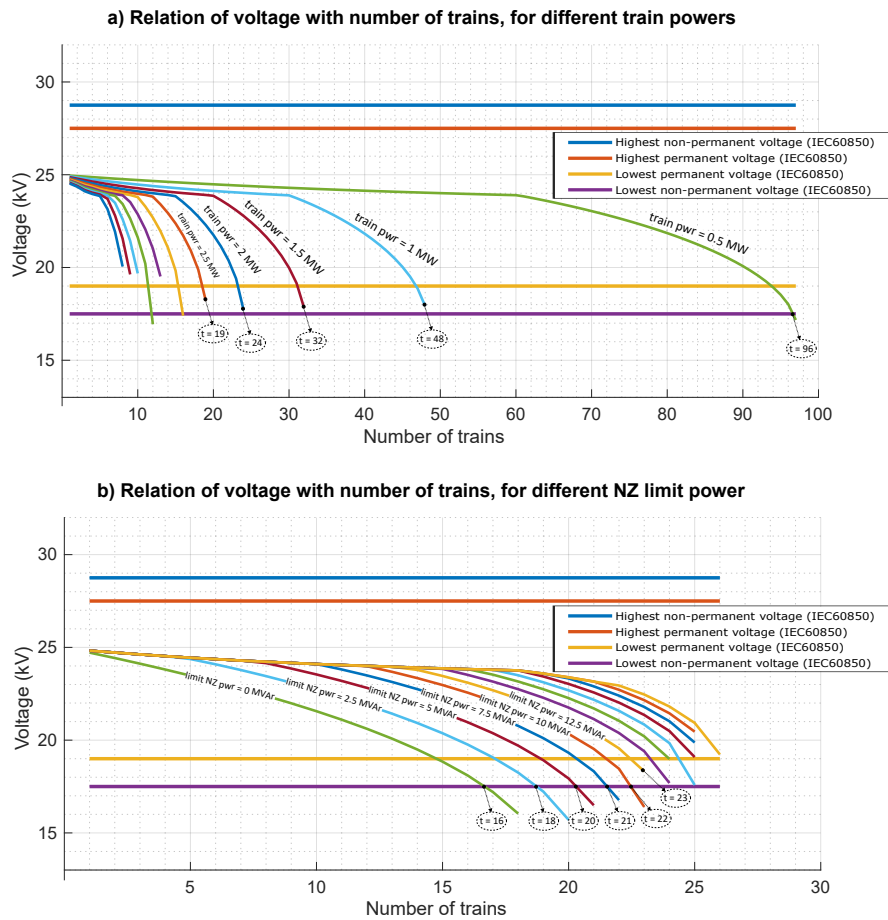


Figure 14. Relation of number of trains ($PF = 0.98$ ind.) with lower voltage in line: (a) variation of active power in each train, for fixed NZ limit power (15 MVA maximum power, as example, visible after 30 trains for 1 MW train power); (b) variation of NZ limit power, for fixed train active power of 2 MW.

From the results of Table 2, it is possible to identify a relation of the maximum number of trains, $N_{trains,max}$, in the line and the power of each train, P_{train} [MW], following (11):

$$N_{trains,max} = K_{NZ,lim} * \frac{1}{P_{train}} \tag{11}$$

In addition, it is possible to estimate the $K_{NZ,lim}$ parameter, since it follows a polynomial function and is dependent on the limit power of the SVC of NZ, P_{NZ} . For the obtained results, this can be extrapolated to the expression in (12):

$$N_{trains,max}(P_{NZ}, P_{train}) = \frac{K_2(P_{NZ})^2 + K_1P_{NZ} + K_0}{P_{train}} \tag{12}$$

where $K_0 = 33.4$, $K_1 = 1.35$ and $K_2 = -0.0252$, for this case study.

The evaluation of the percentage improvement of the railway infrastructure capacity, in Table 2, shows that this improvement is mostly dependent on the NZ reactive power. Specifically, it follows a polynomial trendline, as illustrated in Figure 15.

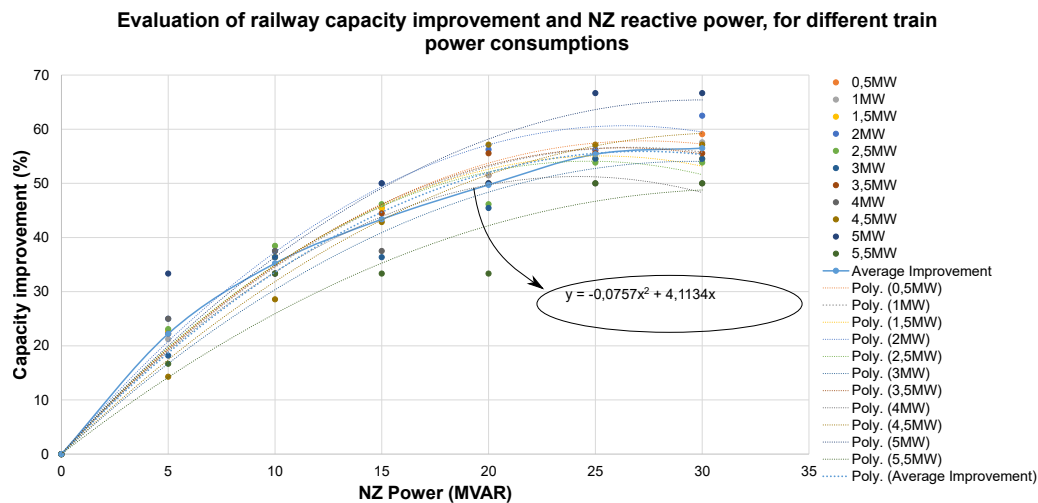


Figure 15. Relation of capacity improvement with the increase of the NZ reactive power. The dots display the Table 2 percentage improvement values; the smaller dot lines present polynomial regression curves from each of those points. The blue dash-dot line (Average improvement) presents a polynomial regression curve from the average of all the improvement values.

The analysis of the trendline shows that, for the considered railway line, the maximum train capacity improvement is around 50% to 60%. However, for higher NZ installed power (above 25 MVAR), it is expected that the capacity improvement will flatten, mostly due to the voltage limitation in the NZ (according to the railway standards, the SVC can not impose a voltage higher than 1.1 p.u).

5.3. Mobile Reactive Power Compensation

Previously, it was considered that the reactive power compensation is performed in NZ. It was visible that the capacity improvement is mostly dependent on the NZ power capability and not in the train power demand.

In this section, the reactive power compensation is performed in each train, where it will be limited by the maximum compensation, which means minimum capacitive power factor. By considering a train operating in any power factor, then the apparent power is given by the following expression:

$$|S| = \frac{P}{PF}, \quad P \in \mathbb{R}_0^+, \quad PF \in]0 \ 1] \quad (13)$$

The variation of the apparent power in relation with the unitary power factor condition is given by:

$$|\Delta S| = \frac{P}{PF} - P \quad (14)$$

If expressed in percentage of P, this variation is only dependent on the power factor:

$$\Delta S[\%] = \left(\frac{1 - PF}{PF} \right) * 100 \quad (15)$$

Figure 16 illustrates the variation of apparent power, $\Delta S[\%]$, for different train power factors.

Similarly to the NZ reactive power compensation algorithm, the mobile reactive power compensation algorithm will adapt the reactive power in one bus (e.g., bus k), in order to minimize the reactive power in another bus (specifically, bus $k - 1$). However, the difference here is that the same algorithm is replicated to all of the trains in the line.

To better illustrate the expected behavior of the compensation scheme, if the train in bus_3 in Figure 11 is considered, this train compensation objective is to have a zero value of reactive power

feeding the $branch_{2 \leftrightarrow 3}$, at bus_2 . This is achieved with the adjustment of power factor, as exemplified in Figure 17, where, from the baseline train reactive power Q_T , this is reduced to Q^* .

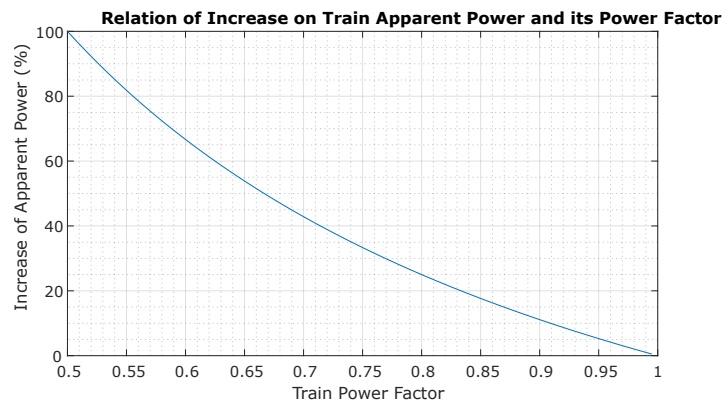


Figure 16. Relation of changing power factor, from unitary one, with an increase of train apparent power.

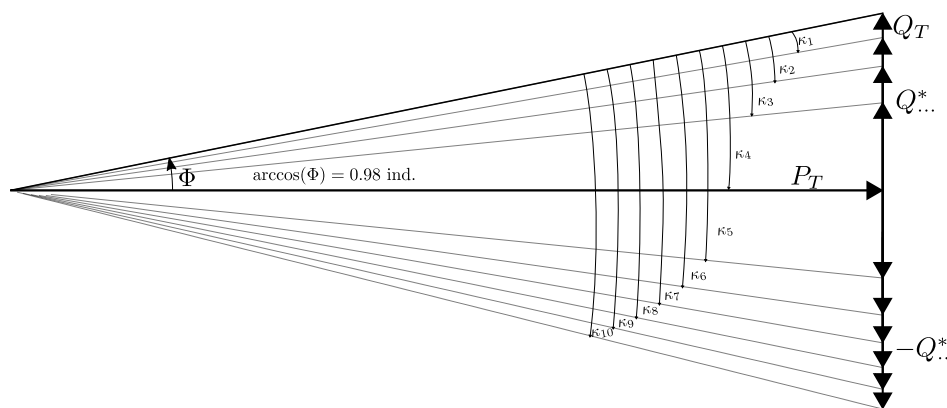


Figure 17. Illustration of the adjustment of power factor for mobile reactive power compensation.

In Figure 17 and, in the following results, the train will start with an inductive power factor (0.98) as a baseline. Furthermore, fixed increments of κ_x will be considered, where $\arccos(\kappa_1) = 0.005$.

Figure 18 presents the results of the mobile reactive power compensation, where the maximum train limit PF is 0.98 cap., in Figure 18a, and follows the different κ_x , in Figure 18b.

In Figure 18b, it is clear that simple adaptation of reactive power in each train will result in an increase in the number of trains. Specifically, changing the PF from 0.98 ind. to 0.94 cap. will result in an increasing in 50% in the number of trains. This result is obtained with the increase of the train apparent power in 6.4% (by using Equation (15) for PF 0.94 cap.). All the results are presented in Table 3.

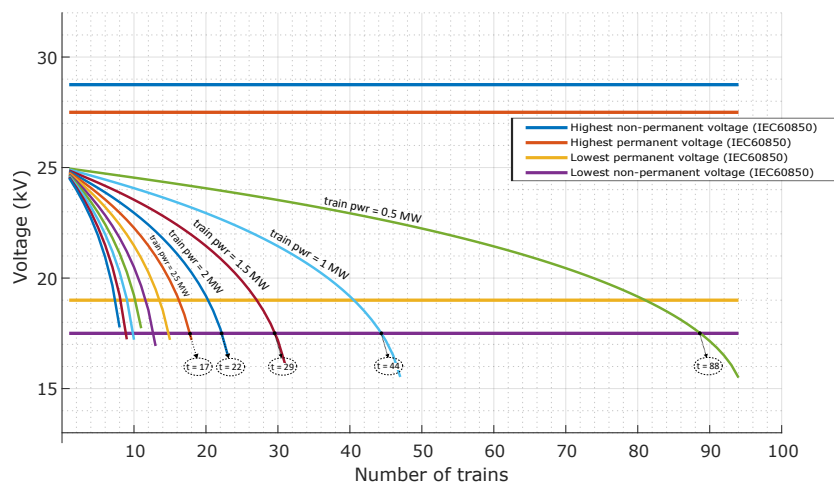
Table 3. Maximum number of trains, for different train power consumptions and for different power factor limit. Note: the percentage improvement from baseline (train PF = 0.98 ind.) is presented in parentheses. As an example, the baseline for $P_T = 2$ MW is 16 trains; then for PF = 0.92 cap., it is possible to have eight more trains (+50% more than baseline).

Train Power Factor	Train Active Power					
	0.5 MW	1 MW	2 MW	3 MW	4 MW	5 MW
0.98 ind.	66 (+0%)	33 (+0%)	16 (+0%)	11 (+0%)	8 (+0%)	6 (+0%)
0.985 ind.	74 (+12%)	37 (+12%)	18 (+13%)	12 (+9%)	9 (+13%)	7 (+17%)
0.99 ind.	77 (+17%)	38 (+15%)	19 (+19%)	12 (+9%)	9 (+13%)	7 (+17%)
0.995 ind.	80 (+21%)	40 (+21%)	20 (+25%)	13 (+18%)	10 (+25%)	7 (+17%)

Table 3. Cont.

Train Power Factor	Train Active Power					
	0.5 MW	1 MW	2 MW	3 MW	4 MW	5 MW
1.00	82 (+24%)	41 (+24%)	20 (+25%)	13 (+18%)	10 (+25%)	8 (+33%)
0.99 cap.	86 (+30%)	43 (+30%)	21 (+31%)	14 (+27%)	10 (+25%)	8 (+33%)
0.98 cap.	88 (+33%)	44 (+33%)	22 (+38%)	14 (+27%)	11 (+38%)	8 (+33%)
0.97 cap.	90 (+36%)	45 (+36%)	22 (+38%)	15 (+36%)	11 (+38%)	9 (+50%)
0.96 cap.	92 (+39%)	46 (+39%)	23 (+44%)	15 (+36%)	11 (+38%)	9 (+50%)
0.94 cap.	95 (+44%)	47 (+42%)	24 (+50%)	16 (+45%)	12 (+50%)	9 (+50%)
0.92 cap.	98 (+48%)	49 (+48%)	24 (+50%)	16 (+45%)	12 (+50%)	10 (+67%)

a) Relation of voltage with number of trains for different train powers (train PF = 0.98 cap.)



b) Relation of voltage with number of trains for different limit train power factors (P = 2 MW)

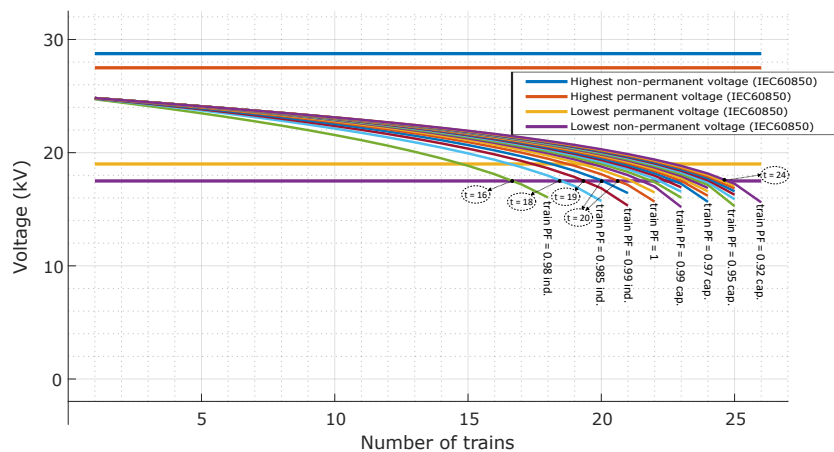


Figure 18. Relation of number of trains (PF = 0.98 ind.) with lower voltage in line: (a) variation of active power in each train, for fixed train PF limit (0.98 cap.); (b) variation of compensation, for fixed train active power of 2 MW.

It is possible to identify a correlation between the capacity improvement, in percentage, and the limit for train power factor. These results are presented in Table 4.

Table 4. Comparison of power factor with apparent power increase and average improvement of railway infrastructure capacity.

Train Power Factor	Power Increase	Capacity Improvement
0.98 ind.	−2.0%	0.0%
0.985 ind.	−1.5%	10.7%
0.99 ind.	−1.0%	15.5%
0.995 ind.	−0.5%	20.2%
1.00	0.0%	23.9%
0.99 cap.	1.0%	28.6%
0.98 cap.	2.0%	32.7%
0.97 cap.	3.1%	39.1%
0.96 cap.	4.2%	40.2%
0.95 cap.	5.3%	41.1%
0.94 cap.	6.4%	44.9%
0.93 cap.	7.5%	46.5%
0.92 cap.	8.7%	51.2%

It can be easily concluded that, if the trains operate with capacitive power factors, the number of trains in the line can be increased. However, the implementation of this strategy should be in compliance with the standard EN 50388-1 [34], by ensuring that the capacitive reactive power compensation made by each train is clipped to zero, once the catenary nominal voltage is reached. In addition, in regenerative mode as stated in the same standard, the voltage is likely to increase and, then, capacitive reactive power compensation must be avoided.

A smart railway framework will take advantage of these results, in order to justify the advantages for either the railway operators and the infrastructure managers. This framework will be covered in the following section.

6. Smart Railway Framework

The advantages of controlling the reactive power flow in the railway electrification were presented in previous sections, both in the reduction of the line losses and in the increase of the railway infrastructure capacity. In this section, the practical implementation of the proposal of this work is discussed. Specifically, a conceptual architecture to implement a reactive power compensation strategy is presented, with the usage of a smart metering framework. This framework targets advantages both for the infrastructure managers and the train operators.

6.1. The Problem of Mobile Reactive Power Compensation

One limitation of the railway infrastructure is in the impossibility of each train to measure the power flowing along the catenary (it is impossible to have current sensors measuring the downstream and upstream currents). The on-board energy measurement and data transmission to ground stations [35] have been implemented in the past few years by railway operators, and the details on this measurement have been actively researched [36].

A reactive power compensation strategy must have accurate measurements on the power flow in the catenary. Specifically, as illustrated in Figure 19, the train T_N must have the knowledge of the power flow at upstream, in the train T_{N-1} node.

This knowledge of the catenary power flow is not an easy task due to several issues:

- It requires the implementation of on-board energy meters in all trains (or in the majority) and in the TPS;
- Requires data reporting to a central station (data gathering);
- It is needed to calculate the power flow in each node and dynamically adapt this calculation mechanism to consider all trains in the traction section (power flow calculation);

- In the case of reactive power compensation strategy, the generated setpoints must be sent to each train (setpoints updating)
- All of these procedures must be made within real-time constraints.

The optimal operation for reactive power compensation will be achieved without delay in the *Data Gathering* → *Power flow calculation* → *Generation of reactive power references* → *Setpoints updating* procedure flow.

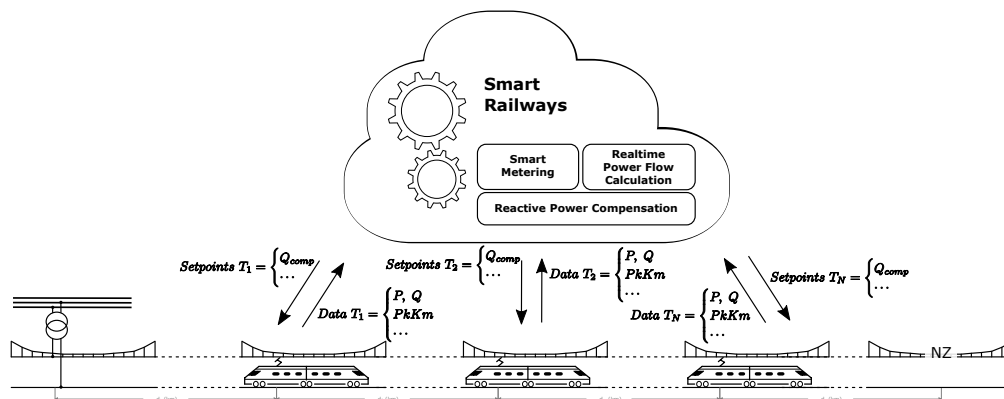


Figure 19. Integration of reactive power compensation in a smart railway framework.

However, in a practical implementation of a reactive power compensation strategy, strategies to avoid non-optimal operation should be adopted. It is clear that the power flow prediction algorithms (that estimate future consumptions) are necessary.

Considering a power flow prediction algorithm that depends on real-time data and can predict a near future, the reactive power compensation algorithm can be more successful to operate in optimal conditions.

Assuming that the smart railways framework is able to predict a time window (as example, 10 s) with a specific accuracy (as example 20% in error) then, in the worst case, the predictor algorithm generates a train reactive power setpoint with a 20% error.

6.2. A Solution for Mobile Reactive Power Compensation

It is necessary to the train to have not only the setpoint of the reactive power, but also the resultant catenary voltage after the compensation. Naturally, the reactive power injected by a train will affect the voltage of the same train; this is a feedback process. The expected and correct voltage value can be used to improve the algorithm in the following way:

- If the train voltage is above the expected voltage, then it means that the amount of reactive power injected is above the optimal value;
 - Then, the on-board reactive power compensation system (viewed as an algorithm that adapts the power factor depending on the desired reactive power value) will reduce the value of reactive power.
- If the train voltage is below the expected, then the on-board reactive power compensation system will increase the injection of reactive power.

A droop-like approach can be used to help stabilize the reactive power control.

This on-board adaptation will follow a droop characteristic curve, as illustrated in Figure 20: the higher the deviation of the voltage and the closer the train is to the NZ, the higher the correction to Q_{comp} .

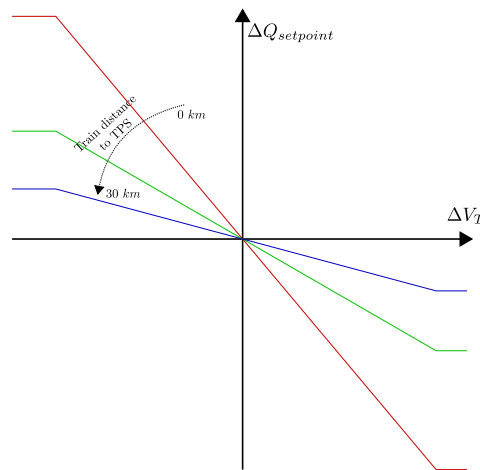


Figure 20. Droop strategy for on-board adjustment. The ΔV_T is the difference between the real train voltage and the expected train voltage. The $\Delta Q_{setpoint}$ is the output of the droop curve, where this value is added to the predicted Q_{comp} .

The slope of the droop characteristic curve might be difficult to obtain. As an example, if all trains have the same droop characteristic curve, it is possible to have a resonance behavior. This train–network interactions and resonance is a well known issue [37], where the converter control loops must be immune to low-frequency oscillation, harmonic resonance, and harmonic instability phenomena (specifically with the tuning of current and voltage control loops, as well as the estimation of the phase angle of the incoming voltage). Therefore, the proposed droop approach most likely reduces a possible low frequency oscillation in the reactive power.

Therefore, in this conceptual implementation, the droop characteristic must be dependent on the distance between the train and the TPS, as well as the number of trains separating a compensation one and the TPS. It is expected that the trains closer to the TPS are requested for a higher contribution of the reactive power, in comparison to the trains closer to the neutral zone.

Considering the example in Figure 21, the usage of the real measured voltage for on-board adaptation of the reactive power will contribute to having an operation closer to the optimal (in comparison with only following the Q_{comp} setpoints).

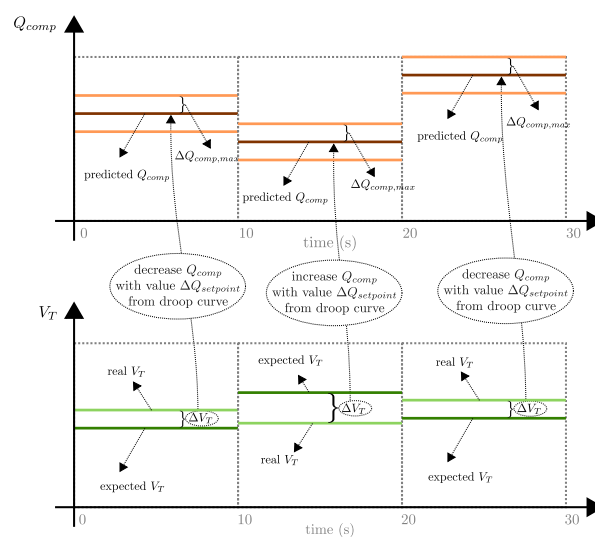


Figure 21. Illustration of the on-board adaptation, supported by the predicted Q_{comp} and $V_{T,estim}$ from the smart railways framework.

6.3. The Path to Reactive Power Compensation

The SVC compensation strategy is based on the inclusion of power electronic devices within the proximity of the NZ. Currently, the compensation strategy is local and does not take into consideration the measurements of the reactive power in the TPS. In this work, a communication channel is considered, where the reactive power is measured in the TPS and used in the NZ to inject reactive power.

The proposed mobile reactive power compensation scheme requires that each train is able to adapt its own power factor. This requirement leaves some of the currently used trains, since the technology used does not allow this level of adaptation. The infrastructure managers can promote modernization of train fleet, with cost reduction of operation for trains able to adapt the reactive power.

As one outcome from UIC International Railway Solutions (IRS) 90930 stakeholders workshop [38], from July 2020 onwards, the European rail sector should implement a new standard for energy metering, which includes the installation of on-board energy metering systems as well as data exchanges on ground [39]. Therefore, the need for smart metering is now closer to being achieved.

Finally, as a preliminary incentive, the billing should accommodate the injection of the reactive power, similarly to the situation happening in certain countries, where the regenerated energy is billed in favor of the railway operator. The clear advantages for the infrastructure managers should allow, in theory, the elimination of the reactive (capacitive) power billing. Further billing strategies should accommodate this effort that the railway operators might take, in order to improve the power quality. The injection of reactive power can be seen as a service that the railway operators can provide.

7. Discussion and Conclusions

In this section, a final discussion and conclusions on the outcomes of this work are presented. This work results from the recent lack of coverage of railway reactive power control in the literature. Specifically, the reactive power control towards increase of railway infrastructure capacity is not an active research topic, from the knowledge of the authors.

From the presented results in this work and as already highlighted in the literature, the increase of railway energy efficiency is clear, not only with the reduction of the reactive power consumption from the transmission/distribution system operator, but also with the reduction of line power losses. The example of Figure 9 illustrates the potential of reduction of catenary power losses up to 50%.

The approach to study the infrastructure capacity improvement is the new hypothesis covered with this work. Specifically, two reactive power compensation strategies are compared, regarding the railway infrastructure capacity. The integration of a static VAR compensation in the neutral zone can increase the railway capacity up to 50%, without its compensation factor depending on the train active power. The second (proposed) compensation strategy considers the integration of the reactive power compensation within each train. With this strategy, it is possible to increase the railway capacity up to 50%, only with an increase of train apparent power below 10%.

The findings in this work were obtained with certain open degrees of freedom, such as each train power consumption, the NZ SVC power limitations, and the maximum capacitive power factor for each train. Certain degrees of freedom were closed with justifications made throughout the article. As an example, the X/R_L ratio was fixed since it depends on the characteristics of the electrification. The line distance was also fixed. It is expected that these two parameters do not affect the railway capacity (in percentage). The other fixed parameter is the distance between each train. It is clear that this corresponds to an ideal situation (in a realistic situation, the train dynamic constraints, journey timetables, signaling, among others, will affect each train position, and the distance between trains will not be all the same). However, only with an extensive statistical analysis is it possible to evaluate if variable train distances result in different results. It is expected, as an example, that, if the majority of trains are more concentrated near the TPS, the resultant minimum voltage will be higher than the fixed distance presented in this work.

Later, in this work, a smart railway framework is proposed, focused on solving the issues regarding this reactive power compensation strategy. A solution is then presented based on a droop controller and a smart metering strategy, which enables the trains to be closer to an optimal point of operation. With this work, the quality of supply in the railway network can be increased, with the adoption of a mobile reactive power compensation strategy based on a smart metering framework.

Author Contributions: For this paper, the investigation as well as the methodology, software development and validation was conducted by V.A.M. under supervision of J.L.A., A.S.C., and A.P.M. The original draft preparation was made by V.A.M. and A.P.M. All authors have read and agreed to the published version of the manuscript.

Funding: This research was funded by FCT (Fundação Ciência e Tecnologia) under grant PD/BD/128051/2016. This research is also associated with the Shift2Rail In2Stempo project (grant 777515).

Conflicts of Interest: The authors declare no conflict of interest.

Abbreviations

The following abbreviations are used in this manuscript:

APQC	Active Power Quality Compensator
HPQC	Hybrid Power Quality Compensator
IRS	International Railway Solutions
MMC	Modular Multilevel Converter
MRPC	Mobile Reactive Power Compensation
NZ	Neutral Zone
PF	Power Factor
PWM	Pulse Width Modulation
RPC	Railway Power Conditioner
SVC	Static VAR Compensator
TPS	Traction Power Substation
UIC	Union Internationale des Chemins de fer—International Union of Railways

References

- IEA. Energy Consumption and CO₂ Emissions Focus on Passenger Rail Services. International Energy Agency (IEA) and International Union of Railways (UIC). Available online: https://uic.org/IMG/pdf/handbook_iaea-uic_2017_web3.pdf (accessed on 24 August 2020).
- Shift2Rail Joint Undertaking. *Shift2Rail Multi-Annual Action Plan, November 2015*; Shift2Rail Joint Undertaking: Brussels, Belgium, 2015.
- Geischberger, J.; Moesters, M. Impact of faster freight trains on railway capacity and operational quality. *Int. J. Transp. Dev. Integr.* **2020**, *4*, 274–285. [[CrossRef](#)]
- Pouryousef, H.; Lautala, P. Hybrid simulation approach for improving railway capacity and train schedules. *J. Rail Transp. Plan. Manag.* **2015**, *5*, 211–224. [[CrossRef](#)]
- Bruni, S.; Bucca, G.; Collina, A.; Facchinetti, A. *Dynamics of the Pantograph Catenary System*; CRC Press: Boca Raton, FL, USA, 2019; pp. 613–647. [[CrossRef](#)]
- Song, Y.; Liu, Z.; Rxnnquist, A.; Navik, P.; Liu, Z. Contact Wire Irregularity Stochastics and Effect on High-speed Railway Pantograph-Catenary Interactions. *IEEE Trans. Instrum. Meas.* **2020**. [[CrossRef](#)]
- Wang, Z.; Cheng, Y.; Mei, G.; Zhang, W.; Huang, G.; Yin, Z. Torsional vibration analysis of the gear transmission system of high-speed trains with wheel defects. *Proc. Inst. Mech. Eng. Part F J. Rail Rapid Transit* **2019**, *234*, 123–133. [[CrossRef](#)]
- IEC 60850. *Railway Applications—Supply Voltages of Traction Systems*; International Electrotechnical Commission (IEC): Geneva, Switzerland, 2007.
- Sauer, P.W. Reactive Power and Voltage Control Issues in Electric Power Systems. In *Power Electronics and Power Systems*; Kluwer Academic Publishers: Boston, MA, USA, 2005; pp. 11–24. [[CrossRef](#)]
- Brenna, M.; Foadelli, F.; Zaninelli, D. *Electrical Railway Transportation Systems*; IEEE Press Series on Power Engineering: Hoboken, NJ, USA, 2018. [[CrossRef](#)]

11. Carson, J.R. Wave Propagation in Overhead Wires with Ground Return. *Bell Syst. Tech. J.* **1926**, *5*, 539–554. [[CrossRef](#)]
12. Pilo, E. Diseño óptimo de la electrificación de Ferrocarriles de alta Velocidad. Ph.D. Thesis, Universidad Pontificia de Comillas, Madrid, Spain, 2003.
13. Aeberhard, M.; Courtois, C.; Ladoux, P. Railway traction power supply from the state of the art to future trends. In Proceedings of the SPEEDAM 2010, Pisa, Italy, 14–16 June 2010; IEEE: New York City, NY, USA, 2010. [[CrossRef](#)]
14. Langerudy, A.T.; Mariscotti, A.; Abolhassani, M.A. Power Quality Conditioning in Railway Electrification: A Comparative Study. *IEEE Trans. Veh. Technol.* **2017**, *66*, 6653–6662. [[CrossRef](#)]
15. Tanta, M.; Pinto, J.G.; Monteiro, V.; Martins, A.P.; Carvalho, A.S.; Afonso, J.L. Topologies and Operation Modes of Rail Power Conditioners in AC Traction Grids: Review and Comprehensive Comparison. *Energies* **2020**, *13*, 2151. [[CrossRef](#)]
16. Luo, A.; Wu, C.; Shen, J.; Shuai, Z.; Ma, F. Railway static power conditioners for high-speed train traction power supply systems using three-phase V/V transformers. *IEEE Trans. Power Electron.* **2011**, *26*, 2844–2856. [[CrossRef](#)]
17. Dai, N.; Wong, M.; Lao, K.; Wong, C. Modelling and control of a railway power conditioner in co-phase traction power system under partial compensation. *IET Power Electron.* **2014**, *7*, 1044–1054. [[CrossRef](#)]
18. Sun, Z.; Jiang, X.; Zhu, D.; Zhang, G. A novel active power quality compensator topology for electrified railway. *IEEE Trans. Power Electron.* **2004**, *19*, 1036–1042. [[CrossRef](#)]
19. Lao, K.; Dai, N.; Liu, W.; Wong, M. Hybrid Power Quality Compensator With Minimum DC Operation Voltage Design for High-Speed Traction Power Systems. *IEEE Trans. Power Electron.* **2013**, *28*, 2024–2036. [[CrossRef](#)]
20. Lao, K.; Wong, M.; Dai, N.Y.; Wong, C.; Lam, C. Analysis of DC-Link Operation Voltage of a Hybrid Railway Power Quality Conditioner and Its PQ Compensation Capability in High-Speed Cophase Traction Power Supply. *IEEE Trans. Power Electron.* **2016**, *31*, 1643–1656. [[CrossRef](#)]
21. Tanta, M.; Pinto, J.G.; Monteiro, V.; Martins, A.P.; Carvalho, A.S.; Afonso, J.L. Deadbeat Predictive Current Control for Circulating Currents Reduction in a Modular Multilevel Converter Based Rail Power Conditioner. *Appl. Sci.* **2020**, *10*, 1849. [[CrossRef](#)]
22. Celli, G.; Pilo, F.; Tennakoon, S.B. Voltage regulation on 25 kV AC railway systems by using thyristor switched capacitor. In Proceedings of the Ninth International Conference on Harmonics and Quality of Power Proceedings (Cat. No.00EX441), Orlando, FL, USA, 1–4 October 2000; Volume 2, pp. 633–638. [[CrossRef](#)]
23. Tan, P.C.; Loh, P.C.; Holmes, D.G. A Robust Multilevel Hybrid Compensation System for 25-kV Electrified Railway Applications. *IEEE Trans. Power Electron.* **2004**, *19*, 1043–1052. [[CrossRef](#)]
24. Fracchia, M.; Courtois, C.; Talibart, A.; Bordignon, P.; Consani, T.; Merli, E.; Bacha, S.; Stuart, M.; Zoeter, K.; Burrarini, G.G.; et al. High Voltage Booster for Railway Applications. World Congress on Railway Research. 2001. Available online: <http://www.railway-research.org/IMG/pdf/278.pdf> (accessed on 24 August 2020).
25. Zanotto, L.; Piovan, R.; Toigo, V.; Gaio, E.; Bordignon, P.; Consani, T.; Fracchia, M. Filter Design for Harmonic Reduction in High-Voltage Booster for Railway Applications. *IEEE Trans. Power Deliv.* **2005**, *20*, 258–263. [[CrossRef](#)]
26. Raygani, S.V.; Moaveni, B.; Fazel, S.S.; Tahavorgar, A. SVC implementation using neural networks for an AC electrical railway. *WSEAS Trans. Circuits Syst.* **2011**, *10*, 173–183.
27. Kulworawanichpong, T. Optimizing AC Electric Railway Power Flows with Power Electronic Control. Ph.D. Thesis, University of Birmingham, Birmingham, UK, 2003.
28. Kulworawanichpong, T.; Goodman, C.J. Optimal area control of AC railway systems via PWM traction drives. *IEE Proc. Electr. Power Appl.* **2005**, *152*, 33–70. [[CrossRef](#)]
29. Tahavorgar, A.; Raygani, S.V.; Fazel, S. Power quality improvement at the point of common coupling using on-board PWM drives in an electrical railway network. In Proceedings of the 2010 1st Power Electronic & Drive Systems & Technologies Conference (PEDSTC), Tehran, Iran, 17–18 February 2010; IEEE: New York, NY, USA, 2010; pp. 412–417. [[CrossRef](#)]
30. Raygani, S.V.; Tahavorgar, A.; Fazel, S.S.; Moaveni, B. Load flow analysis and future development study for an AC electric railway. *IET Electr. Syst. Transp.* **2012**, *2*, 139–147. [[CrossRef](#)]

31. Abril, M.; Barber, F.; Ingolotti, L.; Salido, M.; Tormos, P.; Lova, A. An assessment of railway capacity. *Transp. Res. Part E Logist. Transp. Rev.* **2008**, *44*, 774–806. [[CrossRef](#)]
32. Morais, V.A.; Afonso, J.L.; Martins, A.P. Modeling and Validation of the Dynamics and Energy Consumption for Train Simulation. In Proceedings of the 2018 International Conference on Intelligent Systems (IS), Funchal-Madeira, Portugal, 25–27 September 2018; IEEE: New York, NY, USA, 2018; pp. 288–295. [[CrossRef](#)]
33. Zimmerman, R.D.; Murillo-Sanchez, C.E.; Thomas, R.J. MATPOWER: Steady-State Operations, Planning, and Analysis Tools for Power Systems Research and Education. *IEEE Trans. Power Syst.* **2011**, *26*, 12–19. [[CrossRef](#)]
34. CENELEC EN 50388-1. *Railway Applications—Fixed Installations and Rolling Stock—Technical Criteria for the Coordination between Traction Power Supply and Rolling Stock to Achieve Interoperability—Part 1: General*; CENELEC: Brussels, Belgium, 2017.
35. CENELEC EN 50463-2. *Railway Applications—Energy Measurement on Board Trains*; CENELEC: Brussels, Belgium, 2017.
36. Mariscotti, A. Impact of Harmonic Power Terms on the Energy Measurement in AC Railways. *IEEE Trans. Instrum. Meas.* **2020**, *6731*–6738. [[CrossRef](#)]
37. Hu, H.; Tao, H.; Wang, X.; Blaabjerg, F.; He, Z.; Gao, S. Train–Network Interactions and Stability Evaluation in High-Speed Railways—Part II: Influential Factors and Verifications. *IEEE Trans. Power Electron.* **2018**, *33*, 4643–4659. [[CrossRef](#)]
38. UIC. IRS 90930 (Traction Energy Settlement and Data Exchange). Information Published on 9 October 2018 in the UIC Electronic Newsletter “UIC eNews” Nr 617. Available online: <https://bit.ly/30Urpsw> (accessed on 24 August 2020).
39. Zasiadko, M. New Stage of Energy Measuring for European Rail Sector. 2019 Available online: <https://www.railtech.com/policy/2019/10/28/new-stage-of-energy-measuring-for-european-rail-sector/> (accessed on 24 August 2020).



© 2020 by the authors. Licensee MDPI, Basel, Switzerland. This article is an open access article distributed under the terms and conditions of the Creative Commons Attribution (CC BY) license (<http://creativecommons.org/licenses/by/4.0/>).